Available online at www.sciencedirect.com
ScienceDirect
Trans. Nonferrous Met. Soc. China 28(2018) 1132−1140
Transactions of Nonferrous Metals Society of China
www.tnmsc.cn

Fabrication, microstructures and mechanical properties of ZrO_2 dispersion-strengthened Q345 steel

Bao-an WANG[1], Ning WANG[1,2], Yu-jing YANG[1], Hua ZHONG[1], Ming-zhen MA[1], Xin-yu ZHANG[1], Ri-ping LIU[1]

1. State Key Laboratory of Metastable Materials Science and Technology, Yanshan University, Qinhuangdao 066004, China;
2. CNOOC Research Institute of Oil and Petrochemicals (CRI), Qingdao 266500, China

Received 10 April 2017; accepted 14 April 2018

Abstract: ZrO_2 dispersion-strengthened Q345 steel with different ZrO_2 contents (0%, 0.5% and 1.2%, mass fraction) was fabricated through combining middle frequency induction furnace melting and cored-wire injection technologies. The microstructure and fracture surface morphology of ZrO_2 dispersion-strengthened Q345 steel in casting, normalizing and quenching states were observed using optical microscopy, scanning electron microscopy and transmission electron microscopy. Also, strengthening and fracture mechanisms of the alloys were analyzed. Results showed that the dispersed ZrO_2 particles added into Q345 matrix significantly enhanced its strength, and the main strengthening mechanism was the formation of dislocation cells and pinning effect caused by the addition of ZrO_2 particles. Apart from that, the hard martensite phase, grain refinement and high ZrO_2 particles content also played important roles in strengthening effect. Furthermore, the nanoindentation was also performed to further reveal the strengthening effect and mechanism of dispersed ZrO_2 particles in Q345 steel. Results showed that the hardness of ZrO_2 dispersion-strengthened Q345 steel increased with the increase of ZrO_2 content.

Key words: Q345 steel; ZrO_2 particles; dispersion strengthening; microstructure; mechanical properties

1 Introduction

Mechanical properties of steel always depend on the microstructures of it [1,2]. So, the mechanical properties of steel can be effectively improved by controlling the as-cast microstructure during the production process. Two methods are mainly used to control the as-cast microstructure of steel. One is controlling process parameters of melting and casting such as melt purification, composition, melt temperature, and cooling rate [3]. The other is heat treatment after casting [1,2]. The addition of fine oxide and sulfide particles, and some elements, which will react with molten steel and form finer particles, can promote the heterogeneous nucleation and lead to the grain refinement of steel during melting and casting. Spray−dispersion (SD) method which sprays the fine oxide or carbide particles into steel stream was firstly used to obtain the steel with particle dispersion [4−6]. The addition of some elements such as V, Ti and Nb can further reduce the size of dispersed particles in steel. For example, the addition of 1.0% Nb (molar fraction) can decrease the size of CeO_2 particles to as low as 68 nm in the CeO_2 contained steel. In recent years, the effects of size, density and distribution of dispersed particles and reaction process on the heterogeneous nucleation of steel were researched [7−10].

Dispersion strengthening is a common mechanism in the ferrite steel. And the high-temperature creep properties and radiation effects of the ferrite steel can also be improved by the addition of fine particles [11−13]. So, the dispersion-strengthened ferrite steel has a strong application potential in nuclear industry [14−16]. Several methods are usually used to fabricate dispersion-strengthened steel, such as powder metallurgy [17−19], mechanical alloying [20], chemical immersion method, internal oxidation method, and aluminum thermal synthesis method [21−24]. The powder metallurgy, which produces dispersion-strengthened steel with

Foundation item: Projects (51671166, 51434008) supported by the National Natural Science Foundation of China; Project (2013CB733000) supported by the National Basic Research Program of China
Corresponding author: Ming-zhen MA; Tel: +86-335-8064504; Fax: +86-335-8074545; E-mail: mz550509@ysu.edu.cn
DOI: 10.1016/S1003-6326(18)64750-8

excellent high-temperature strength and creep properties, is one of the most widely used methods [25−30].

In recent years, cored-wire injection technology is usually used to fabricate alloys or composites due to its simple process. However, there is a lack in study on the fabrication of dispersion-strengthened steel using this method.

The Q345 steel was wildly used in low-pressure vessels, oil tanks, vehicles, cranes, mining machinery, power plants, and bridges due to its excellent mechanical and welding properties. In recent years, the oxide particles, such as ZrO_2, TiO_2, Al_2O_3, CeO_2, Y_2O_3, WO_2 and ThO, are usually used as the dispersion strengthening phase in the Q345 steel. Among these particles, the ZrO_2 particle exhibits some excellent properties, such as high melting point of 2710 °C, low free energy of −1042.15 kJ/mol, high stiffness coefficient of 200 GPa, high hardness with Mohs rating of 6.5, high density of 5.68 g/cm^3, good thermal stability, high density and low price. So, the ZrO_2 particle should be a favorable dispersion strengthening phase for the Q345 steel. However, the result concerning the ZrO_2 dispersion-strengthened Q345 steel is rare.

In this work, the ZrO_2 particle was selected as the dispersion strengthening phase to fabricate ZrO_2 dispersion-strengthened Q345 steel using cored-wire injection technology. Microstructures and mechanical properties of ZrO_2 dispersion-strengthened Q345 steel after casting, normalizing and water quenching were investigated. Furthermore, the strengthening mechanism of these steels was also discussed.

2 Experimental

Q345 steel, ZrO_2 particles, and industrial pure iron powders were used as raw materials. The sizes of ZrO_2 particle and iron powder were about 45 μm, and Table 1 presents the chemical compositions of the raw materials.

500 g iron matrix powders containing 20% (mass fraction) ZrO_2 particles were mixed using a QM−3SP04L type planetary mill. The mass ratio of balls to powder was fixed to 1:1. Milling was performed for 5 h in the argon environment and the rotation rate was 400 r/min. The mixed powders were put into an iron pipe with a diameter of 6 mm and air-dried at 300 °C.

The ZrO_2 dispersion-strengthened Q345 steel samples with 0%, 0.5% and 1.2% (mass fraction) ZrO_2 were prepared by melting the Q345 ingot and mixed powders in a middle-frequency induction furnace. The melting and pouring temperatures were approximately 1600 °C. The normalizing process contained two-stage heating and holding and then air cooling to room temperature. The first stage was heating the samples from room temperature to 850 °C with a rate of 20 °C/min, and holding for 10 min. The second stage was heating the samples from 850 to 910 °C with a rate of 10 °C/min, and holding for 30 min. The quenching process contained also two-stage heating and holding and then water quenching to room temperature. The first stage was the same with the normalizing process. The second stage was heating the samples from 850 to 925 °C with a rate of 10 °C/min, and holding for 30 min.

The microstructures of samples were examined by optical microscopy (OM) and transmission electron microscopy (TEM). TEM specimens were prepared by mechanical grinding to a thickness of approximately 50 μm, followed by thinning using a twinjet electro-polishing in a solution of 7% acetic acid and 93% glacial acetic acid (volume fraction) at 18 °C, and the voltage of 22 V. Tensile tests were performed using an Instron-5982 machine at a tensile speed of 0.008 mm/s. Figure 1 shows the size of tensile specimens. The fracture surface after tensile tests was observed by scanning electron microscopy (SEM). In the nanoindentation test, the Hysitron triboindenter (TI−900) was employed with the load up to the maximum of 8 mN. The surface finish of specimen was about 50 nm, and the data were averaged.

3 Results and discussion

Figure 2 shows the OM images of as-cast ZrO_2 particle dispersion-strengthened Q345 steel with different ZrO_2 contents. The pearlite (black phase) and coarse ferrite (white phase) were observed in the as-cast Q345 steel without ZrO_2 (Fig. 2(a)). 0.5% ZrO_2 addition changed the morphology of ferrite into irregular multilateral and flake shapes, and refined the grain of ferrite (Fig. 2(b)). Increasing the content of ZrO_2 to 1.2%, the size of ferrite grains was further reduced, and the content of pearlite was increased (Fig. 2(c)).

Figure 3 shows the OM images of as-normalized ZrO_2 particle dispersion-strengthened Q345 steel with different ZrO_2 contents. Compared with the as-cast Q345

Table 1 Chemical compositions of Q345 steel, pure iron powders and ZrO_2 particles (mass fraction, %)

Material	C	Si	Mn	Ni	Cr	Cu	P	S	Fe	ZrO_2	Impurity
Q345 steel	0.19	0.27	0.56	0.21	Trace	Trace	Trace	Trace	Bal.	−	
Fe powder	−	−	−	−	−	−	−	−	99.99	−	Bal.
ZrO_2 particle	−	−	−	−	−	−	−	−	−	98.8	Bal.

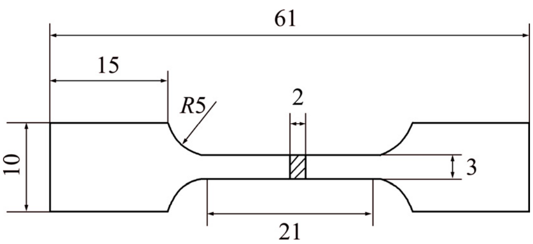

Fig. 1 Sizes of tensile specimens (unit: mm)

steel, the as-normalized Q345 steel exhibited finer ferrite (Fig. 3(a)). The size of ferrite and pearlite decreased with increasing ZrO_2 content, as shown in Figs. 3(b) and (c). Compared with the casting process, the normalizing treatment has a higher cooling rate. And the high cooling rate suppressed the precipitation of carbides along austenite grain boundaries. So, ZrO_2 particle addition and normalizing treatment could lead to the occurrence of grain refinement and improvement of uniformity in the Q345 steel.

Figure 4 shows the OM images of as-quenched ZrO_2 particle dispersion-strengthened Q345 steel with different ZrO_2 contents. The martensite with strip or plate shapes was observed in all as-quenched samples. The Q345 is a kind of low-carbon steel, and the martensite always exhibited strip or plate shapes when the carbon content in the austenite was less than 0.2%. The size of martensite in as-quenched samples decreased with increasing ZrO_2 content. The ZrO_2 particle could inhibit the grain coarsening of austenite during solid-solution treatment, thereby refining the grain of martensite.

Figure 5 shows mechanical properties of as-cast Q345 steel and ZrO_2 particle dispersion-strengthened

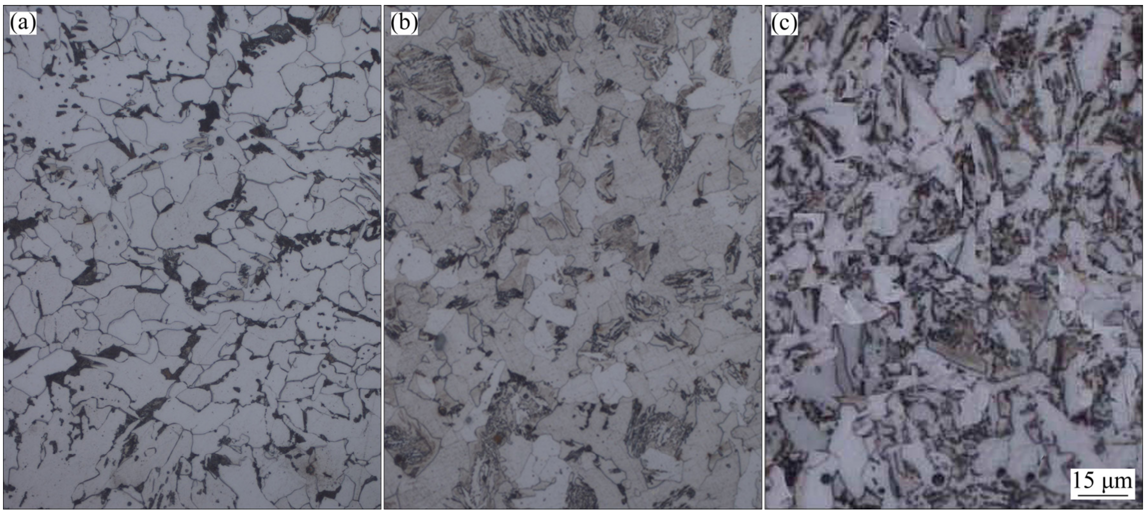

Fig. 2 OM micrographs of as-cast ZrO_2 particle dispersion-strengthened Q345 steel with various ZrO_2 contents: (a) 0%; (b) 0.5%; (c) 1.2%

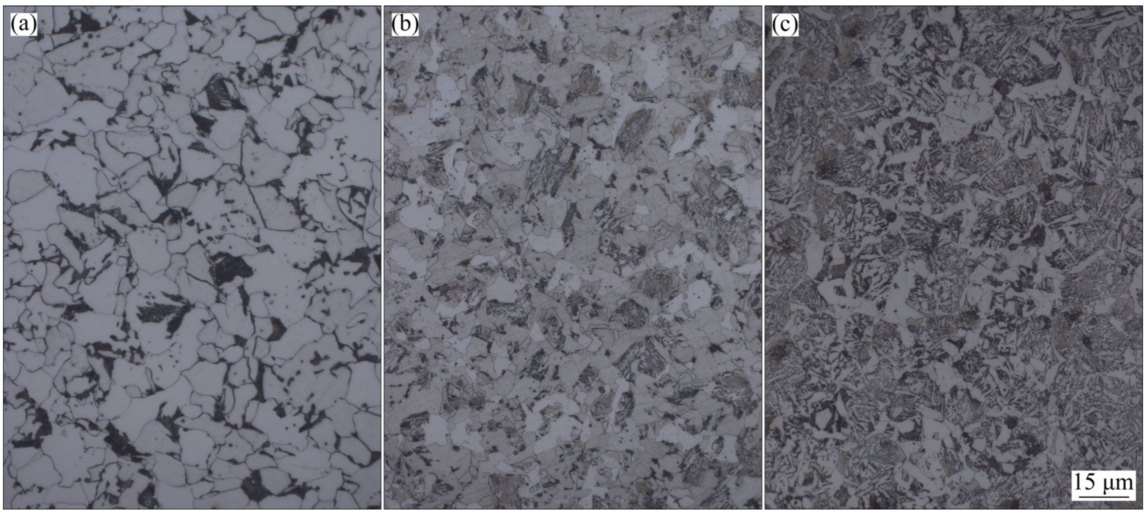

Fig. 3 OM micrographs of as-normalized ZrO_2 particle dispersion-strengthened Q345 steel with various ZrO_2 contents: (a) 0%; (b) 0.5%; (c) 1.2%

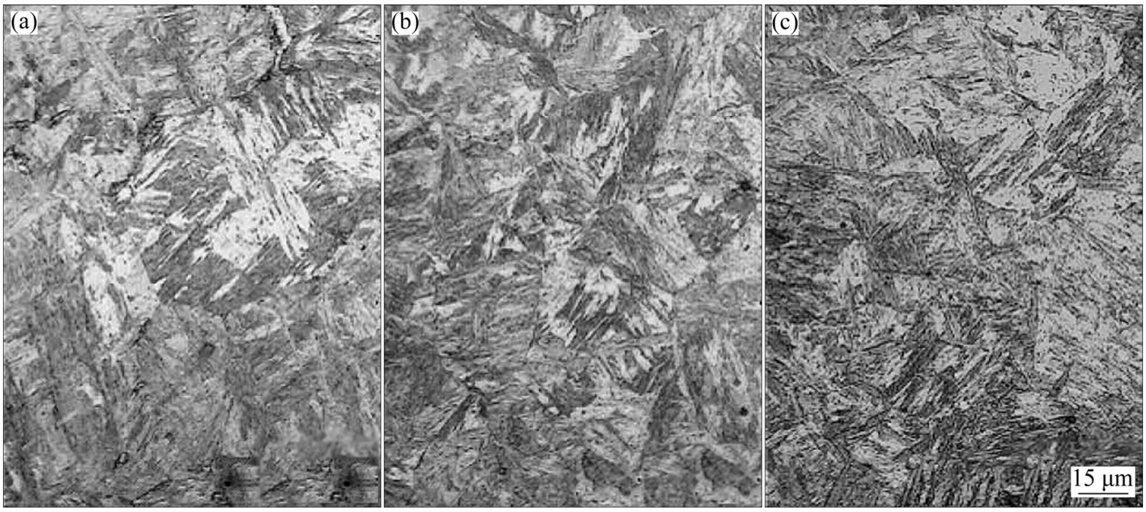

Fig. 4 OM micrographs of as-quenched ZrO_2 particle dispersion-strengthened Q345 steel with various ZrO_2 contents: (a) 0%; (b) 0.5%; (c) 1.2%

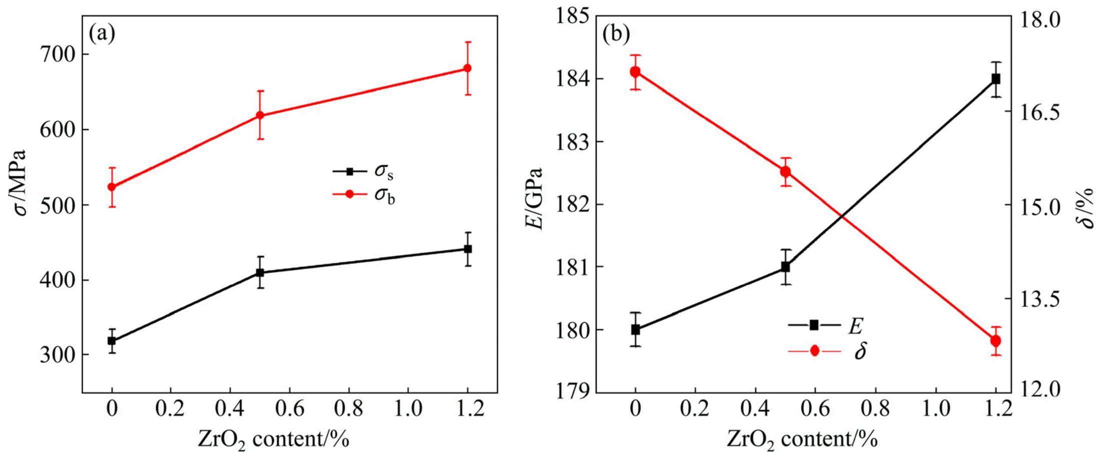

Fig. 5 Mechanical properties of as-cast ZrO_2 particle dispersion-strengthened Q345 steel with different ZrO_2 contents: (a) Yield strength and ultimate tensile strength; (b) Elastic modulus and elongation

Q345 steel with different ZrO_2 contents. The elastic modulus and strength of as-cast samples increased with increasing ZrO_2 content. The elastic modulus, ultimate strength (UTS) and 0.2% yield strength (YS) of 1.2% ZrO_2 particle dispersion-strengthened Q345 steel reached 184 GPa, 441 MPa and 680 MPa, respectively. Conversely, the ductility of as-cast samples decreased with increasing ZrO_2 content. Encouragingly, the as-cast 1.2% ZrO_2 particle dispersion-strengthened Q345 steel still had total elongation (EL) of approximately 12%.

Figure 6 shows mechanical properties of as-normalized Q345 steel and ZrO_2 particle dispersion-strengthened Q345 steel with different ZrO_2 contents. The elastic modulus and strength of as-normalized samples increased with increasing ZrO_2 content. The elastic modulus, UTS and YS of 1.2% ZrO_2 particle dispersion-strengthened Q345 steel reached 194 GPa, 538 MPa and 845 MPa, respectively. But, the ductility of as-normalized samples decreased with increasing ZrO_2 content. The EL of as-normalized 1.2% ZrO_2 particle dispersion-strengthened Q345 steel reached 15.5%.

Compared with as-cast samples, as-normalized samples with the same composition showed both high strength and ductility. Thus, the normalizing treatment could effectively improve mechanical properties of as-cast ZrO_2 particle dispersion-strengthened Q345 steel. The key reason was the refined grain sizes of ferrite and pearlite after normalizing treatment (Fig. 3).

Figure 7 shows mechanical properties of as-quenched Q345 steel and ZrO_2 particle dispersion-strengthened Q345 steel with different ZrO_2 contents. The elastic modulus and strength of as-quenched samples increased with increasing ZrO_2 content. The elastic modulus, UTS, and YS of 1.2% ZrO_2 particle dispersion-strengthened Q345 steel reached 196 GPa, 955 MPa and 1398 MPa, respectively. While the ductility of

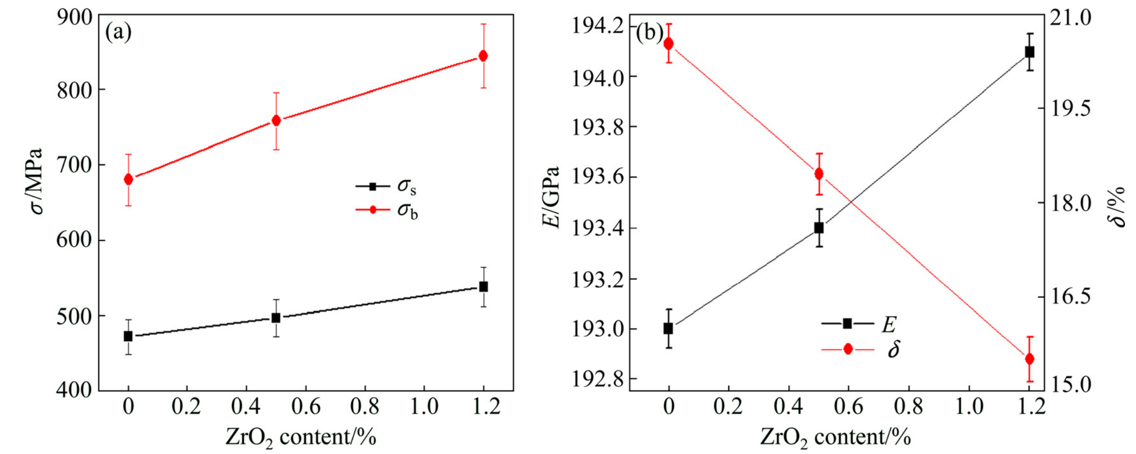

Fig. 6 Mechanical properties of as-normalized ZrO_2 particle dispersion-strengthened Q345 steel with different ZrO_2 contents: (a) Yield strength and ultimate tensile strength; (b) Elastic modulus and elongation

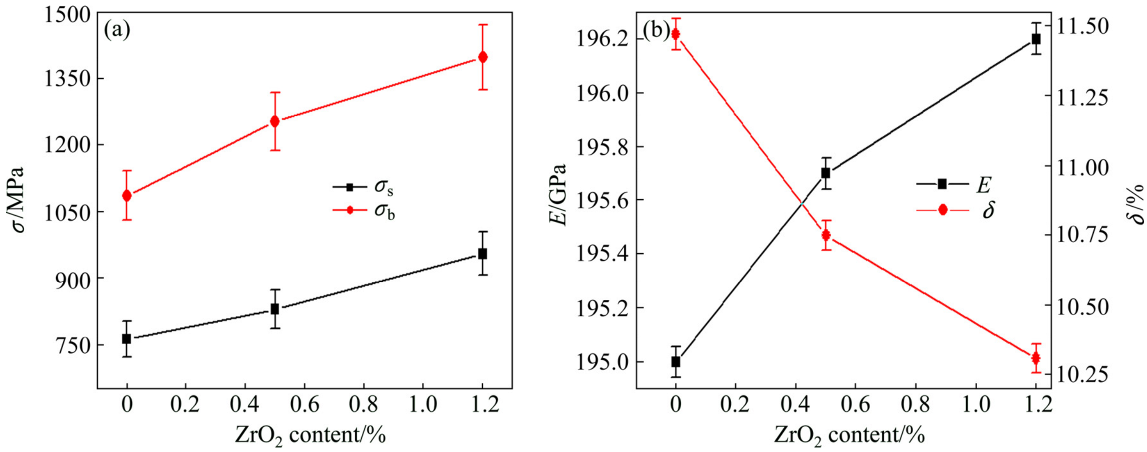

Fig. 7 Mechanical properties of as-quenched ZrO_2 particle dispersion-strengthened Q345 steel with different ZrO_2 contents: (a) Yield strength and ultimate tensile strength; (b) Elastic modulus and elongation

as-quenched samples decreased with increasing ZrO_2 content. The EL of as-quenched 1.2% ZrO_2 particle dispersion-strengthened Q345 steel reached 10%.

It is well known that the lamellar-shape martensite in high-carbon steels after quenching treatment is a kind of hard brittle phase. Thus, high-temperature tempering is usually employed after quenching treatment for high-carbon steels to improve ductility at the expense of strength. So, it is hard for high-carbon steels to have both high strength and ductility. It was found that the martensite with the strip and/or plate shapes could exhibit both high strength and ductility without tempering [31]. So, the as-quenched Q345 steel with striped and plated martensite in this work showed excellent strength and ductility.

Figure 8 shows the TEM micrographs of as-normalized 1.2% ZrO_2 particle dispersion-strengthened Q345 steel and ZrO_2-free Q345 steel after tensile test. The tensile deformation led to the formation of dislocation (Fig. 8(c)). However, the density of dislocation in ZrO_2 particle dispersion-strengthened Q345 steel (Figs. 8(a) and (c)) was higher than that of the ZrO_2-free Q345 steel. So, the addition of ZrO_2 particles increased the density of dislocation in the Q345 steel. The high density of dislocation was observed in the matrix near the matrix−particle interface. In order to ensure the comparability of dislocation density between ZrO_2 strengthened and free Q345 steel, the diffraction spots along the direction of $\vec{g}_{110}$ were inserted into the Figs. 8(a) and (c). For particle reinforced metal matrix composites, the high dislocation density could be obtained in the matrix after heat treatments owing to the large difference in thermal expansion between the matrix and reinforcing phase. The large difference in thermal expansion between Fe and ZrO_2 particles results in the generation of dislocations in the as-normalized samples during cooling from 910 °C in air. Thus, the as-normalized ZrO_2 particle dispersion-strengthened Q345 steel exhibited higher dislocation strengthening effect. Furthermore, the grain coarsening of Q345 steel was inhibited by the addition of ZrO_2 particle (Figs. 2, 3 and 4). So, compared with Q345 steel, the ZrO_2 particle dispersion-strengthened Q345 steel exhibited simultaneously higher boundary strengthening effect. In addition, the second phase strengthening effect of ZrO_2 particle dispersion-strengthened Q345 steel also increased with increasing ZrO_2 content. Thus, the high strength of as-normalized 1.2% ZrO_2 particle dispersion-strengthened Q345 steel was attributed to the hard martensite phase, grain refinement, high density of dislocations and high dispersed ZrO_2 particle content.

Figure 9 shows the tensile fracture morphologies of as-normalized ZrO_2 particle dispersion-strengthened Q345 steel with different ZrO_2 contents. The deep dimples in the Q345 steel clearly exhibited a typical ductile fracture (Fig. 9(a)). With increasing ZrO_2 content, more fine dimples were observed in as-normalized ZrO_2 particle dispersion-strengthened Q345 samples. These fine dimples were caused by the ZrO_2 addition induced grain refinement. The 1.2% ZrO_2 particle dispersion-strengthened Q345 steel also exhibited the ductile fracture features of dimples and shear zones. The rupture model consisted of a fracture that occurs through the formation and coalescence of microvoids crossing the entire sample. The fracture morphologies of ZrO_2 particle dispersion-strengthened Q345 steel also indicated the strong bond between the matrix and ZrO_2 particle even at high tensile stresses.

Figure 10 shows the load−displacement curves of nanoindentation performed at a load of 8 mN in ZrO_2

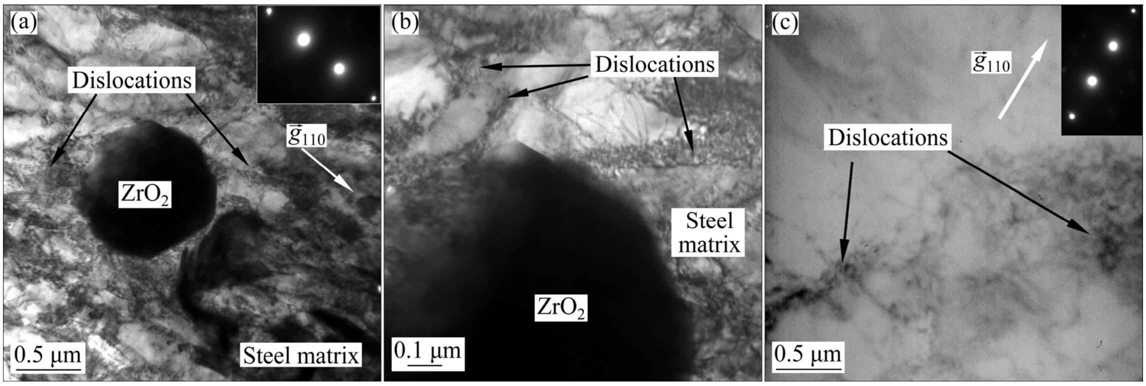

Fig. 8 TEM micrographs of as-normalized 1.2% ZrO_2 particle dispersion-strengthened Q345 steel in low (a) and high (b) magnification, and Q345 steel (c) after tensile test

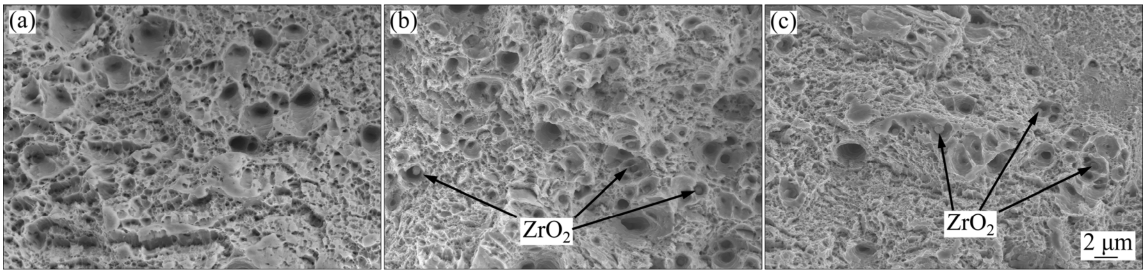

Fig. 9 Fracture morphologies of as-normalized ZrO_2 particle dispersion-strengthened Q345 steel with various ZrO_2 contents: (a) 0%; (b) 0.5%; (c) 1.2%

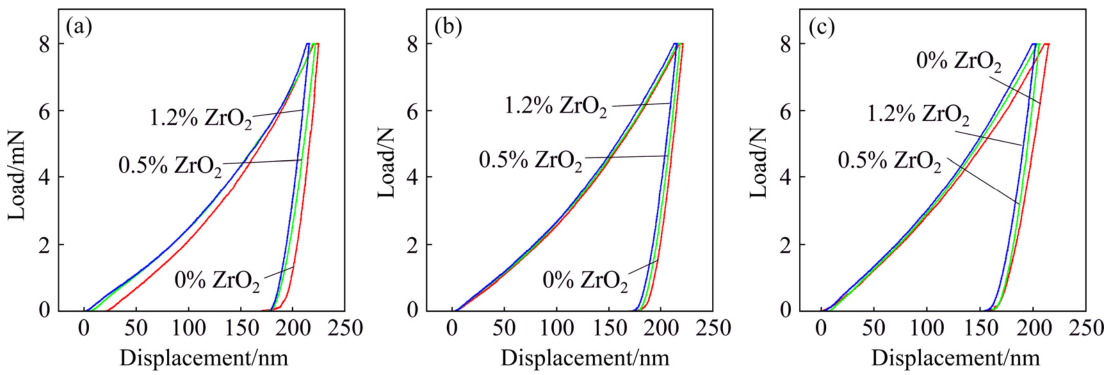

Fig. 10 Load−displacement curves of nanoindentation in ZrO_2 particle dispersion-strengthened Q345 steel in different states: (a) As-cast; (b) As-normalized; (c) As-quenched

particle dispersion-strengthened Q345 steel with different ZrO_2 contents and states. For the samples in each state, the indentation depth decreased with increasing ZrO_2 content. To reveal the relationship between nanoindentation hardness and indentation depth in ZrO_2 particle dispersion-strengthened Q345 steel, all load−displacement curves were transformed into hardness−displacement curves. The Oliver−Pharr method [32] and geometric parameters of Berkovick were used to calculate the depth−dependent values of nanoindentation hardness. The nanoindentation hardness (H) of ZrO_2 particle dispersion-strengthened Q345 steel can be expressed by

$$H=\frac{P}{24.56(h_c+0.06R)} \tag{1}$$

where P is the load, h_c is the displacement, and R is the radius of the tip (450 nm in this work).

The curves for the nanoindentation hardness versus displacement of ZrO_2 particle dispersion-strengthened Q345 steel are shown in Fig. 11. The relationship of the parameters of nanoindentation and those of the tensile test is

$$1/E_r=(1-v^2/E)+(1-v_i^2/E_i) \tag{2}$$

where E_r is the modulus of nanoindentation, E is the elastic modulus of materials, E_i is the elastic modulus of squeeze head, v is the Poisson ratio of materials, and v_i is the Poisson ratio of squeeze head. The modulus of nanoindentation, nanoindentation hardness and indentation depth of ZrO_2 particle dispersion-strengthened Q345 steel are displayed in Table 2. The nanoindentation hardness of ZrO_2 particle dispersion-strengthened Q345 steel increased with ZrO_2 content. For as-cast samples, the hardness reached the maximum at the displacement of 215−225 nm. The final hardness of as-cast samples increased with increasing ZrO_2 content, and the 1.2% ZrO_2 particle dispersion-strengthened Q345 steel had a final hardness of approximately 5.23 GPa. Whereas the final displacement of the as-cast samples decreased with increasing ZrO_2 content, and that of the 1.2% ZrO_2 particle dispersion-strengthened Q345 steel decreased to 214.745 nm (Fig. 11(a)). For as-normalized and as-quenched samples, the trends of hardness varying with displacement are similar to those of as-cast samples. The hardness of as-normalized and as-quenched 1.2% ZrO_2 particle dispersion-strengthened Q345 steel increased to 5.59 and 5.62 GPa, respectively. But the displacement of as-normalized and as-quenched 1.2% ZrO_2 particle dispersion-strengthened Q345 steel decreased to 206.506 and 202.797 nm, respectively.

For the ZrO_2 particle dispersion-strengthened Q345 steel under the same heat treatment process, the

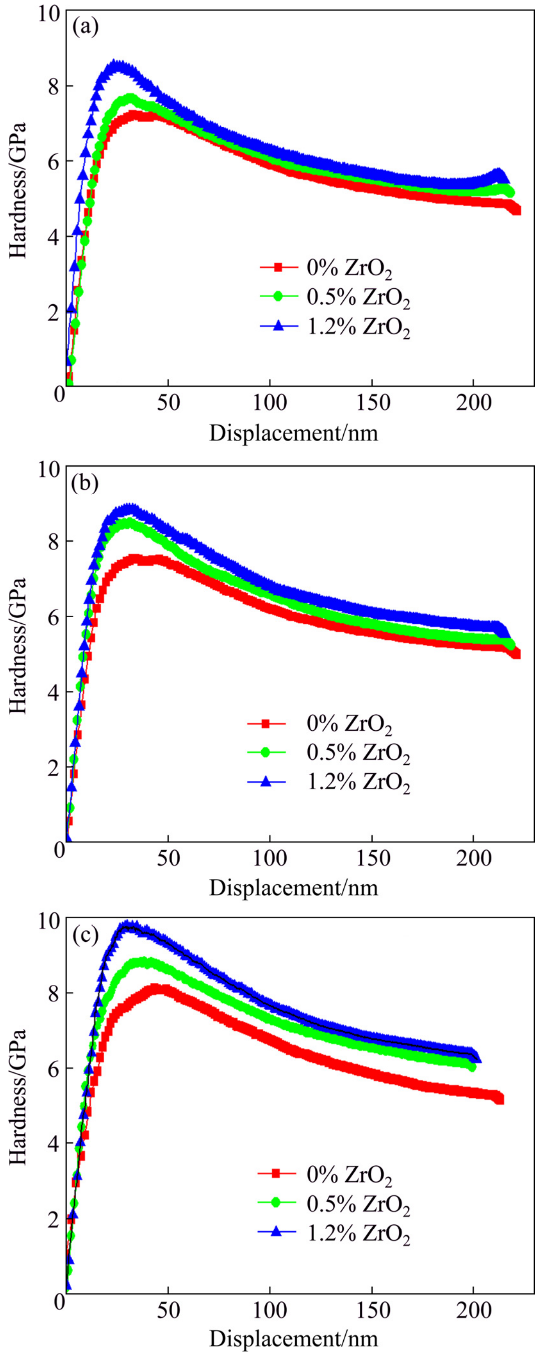

Fig. 11 Hardness–displacement curves of nanoindentation in ZrO_2 particle dispersion-strengthened Q345 steel in different states: (a) As-cast; (b) As-normalized; (c) As-quenched

hardness increased but the final displacement decreased with increasing ZrO_2 content. The addition of ZrO_2 particle led to the higher density of dislocation in the steel matrix (Fig. 8). So, the hardness and deformation capacity of steel matrix respectively increased and decreased with increasing ZrO_2 content.

For the ZrO_2 particle dispersion-strengthened Q345 steel with same ZrO_2 content, the hardness and final displacement depended on the heat treatment. Compared with the as-cast samples, the as-normalized samples

Table 2 Nanoindentation modulus, hardness and indentation depth of ZrO_2 particle dispersion-strengthened Q345 steel with different ZrO_2 contents and states

State	$w(ZrO_2)$=0%			$w(ZrO_2)$=0.5%			$w(ZrO_2)$=1.2%		
	E_r/GPa	H/GPa	Depth/nm	E_r/GPa	H/GPa	Depth/nm	E_r/GPa	H/GPa	Depth/nm
As-cast	169	4.68	224.703	179	4.87	220.723	181	5.23	214.974
As-normalized	170	4.82	221.646	179.3	4.93	218.621	181.1	5.59	206.506
As-quenched	172	4.95	215.444	179.8	5.26	215.519	181.5	5.62	202.797

showed higher hardness. Furthermore, the maximum hardness values of the as-normalized samples located at the displacement of 207−222 nm, shorter than that in the as-cast samples. These phenomena can be attributed to the occurrence of grain refinement and improvement of uniformity in the samples after normalizing treatment (Figs. 2 and 3). The hardnesses of as-quenched samples were higher than those of as-cast and as-normalized samples with the same ZrO_2 content, as shown in Fig. 11(c). The martensite phase with higher hardness was obtained in the ZrO_2 particle dispersion-strengthened Q345 steel after quenching treatment (Fig. 4). So, the as-quenched ZrO_2 particle dispersion-strengthened Q345 steel exhibited the highest hardness, and the strengthening mechanism of these samples included martensite phase, boundary, dislocations, and dispersed ZrO_2 particles strengthening.

It was found that, for the same sample, the modulus tested by nanoindentation was lower than that tested by tensile experiment. This phenomenon can be attributable to the nonuniformity of mechanical properties in the materials [33]. However, the modulus of both tensile test and nanoindentation increased with increasing ZrO_2 content.

4 Conclusions

1) The addition of ZrO_2 to the Q345 steel caused the grain refinement of cast alloy. Furthermore, the sizes of ferrite, pearlite, and martensite in normalized and/or quenched Q345 were also refined by the ZrO_2 addition.

2) The high density of dislocations was observed near particles−matrix interface in the ZrO_2 particle dispersion-strengthened Q345 steel due to the large difference in thermal expansion between Q345 matrix and ZrO_2 reinforcing phase.

3) The mechanical properties of Q345 steel were improved by quenching treatment and ZrO_2 addition. The as-quenched 1.2% ZrO_2 particle dispersion-strengthened Q345 steel showed balanced mechanical properties, including high strength, high elastic modulus, high micro-hardness and reasonable ductility.

4) The strengthening mechanism of as-quenched ZrO_2 particle dispersion-strengthened Q345 steel included integrated strengthening from hard martensite phase, plenty of boundaries, high dislocations density and dispersed ZrO_2 particles. And the fracture was still ductile.

References

[1] MAKI T. Current state and future prospect of microstructure control in steels [J]. Tetsu To Hagane−Journal of the Iron and Steel Institute of Japan, 1995, 81(11): N547−555.

[2] XIE Jian-xin. Advance on microstructure control strengthening technology for structure steels [J]. Special Steel, 1999, 20(3): 7−12.

[3] XU Kuang-di, XIAO Li-jun. Deoxidation and inclusion control in special steel refining [J]. Iron and Steel, 2012, 47(10): 1−13.

[4] HASEGAWA M, TAKESHITA K, FUKUMI J, SASSA K. Study on CaS-dispersed steel produced by spray-dispersion method [J]. Tetsu To Hagane−Journal of the Iron and Steel Institute of Japan, 1978, 64(14): 126−135.

[5] HASEGAWA M, TAKESHITA K, WATANABE S. Oxide dispersion strengthened nickel and nichrome by means of the spray-dispersion method [J]. Tetsu To Hagane−Journal of the Iron and Steel Institute of Japan,1982, 68(8): 130−137.

[6] HASEGAWA M, TAKESHITA K. Strengthening of steel by spray-dispersion of fine oxide particles [J]. Tetsu To Hagane−Journal of the Iron and Steel Institute of Japan, 1977, 63(2): 96−104.

[7] OKUDA T. Control of oxide particle size and recrystallized grain structure in oxide dispersion strengthened ferritic steel [J]. Tetsu To Hagane−Journal of the Iron and Steel Institute of Japan,1997, 83(12): 25−30.

[8] HIROKI O, HIDEAKI S. Precipitation and dispersion control of MnS by deoxidation products of ZrO_2, Al_2O_3, MgO and MnO-SiO_2 particles in Fe−10 mass% Ni alloy [J]. ISIJ International, 2006, 46(4): 480−489.

[9] ∅YSTEIN G, LEIV K，CASPER V D E, GABRIELLA T. Microstructure control of steels through dispersoid metallurgy using novel grain refining alloys [J]. ISIJ International, 2006, 46(6): 824−831.

[10] NAKAJIMA K, OHTA H, SUITO H, JÖNSSON P. Effect of oxide catalyst on heterogeneous nucleation in Fe−10mass%Ni alloys [J]. ISIJ International, 2006, 46(6): 807−813.

[11] MIAO Yin-bin, MO Kun, CUI Bai, CHEN Wei-ying, MILLER M K, POWERS K A, MCCREARY V, GROSS D, ALMER J, ROBERTSON I M, STUBBINS J F. The interfacial orientation relationship of oxide nanoparticles in a hafnium-containing oxide dispersion-strengthened austenitic stainless steel [J]. Materials Characterization, 2015, 101: 136−143.

[12] GWON Jin-han, KIM Jeoung-han, LEE Kee-ahn. Effects of cryomilling on the microstructures and high temperature mechanical properties of oxide dispersion strengthened steel [J]. Journal of Nuclear Materials, 2015, 459: 205−216.

[13] LIU Tong, WANG Lin-bo, WANG Chen-xi, SHEN Hai-long, ZHANG Hong-tao. Feasibility of using $Y_2Ti_2O_7$ nanoparticles to fabricate high strength oxide dispersion strengthened Fe−Cr−Al steels [J]. Materials & Design, 2015, 88: 862−870.

[14] NGANBE M, HEILMAIER M. Modelling of particle strengthening in the γ' and oxide dispersion strengthened nickel-base superalloy PM3030 [J]. Materials Science and Engineering A, 2004, 387−389: 609−612.
[15] LI Shao-fu, ZHOU Zhang-jian, LI Ming, WANG Man, ZHANG Guang-ming. Microstructure characterization and tensile properties of 18Cre4Al-oxide dispersion strengthened ferritic steel [J]. Journal of Alloys and Compounds, 2015, 648: 39−45.
[16] SURYANARAYANA C, IVANOV E, BOLDYREV V V. The science and technology of mechanical alloying [J]. Materials Science and Engineering A, 2001, 304−306: s151−s158.
[17] LIU Long-fei, WU Shu-sen, CHEN Yang, LÜ Shu-lin. Oxidation behavior of RE-modified nickel-based superalloy between 950 °C and 1150 °C in air [J]. Transactions of Nonferrous Metals Society of China, 2016, 26(4): 1163−1169.
[18] XIAO Zuo-an, TANG Di-yong, FAN Jin-hang, XIAO Wei, WANG Di-hua. Coating titanium on carbon steel by in-situ electrochemical reduction of solid TiO_2 layer [J]. Transactions of Nonferrous Metals Society of China, 2017, 27(1): 134−140.
[19] HE P, LIU T, MOESLANG A, LINDAU R, ZIEGLER R, HOFFMANN J, KURINSKIY P, COMMIN L, VLADIMIROV P, NIKITENKO S, SILVEIR M. XAFS and TEM studies of the structural evolution of yttrium-enriched oxides in nanostructured ferritic alloys fabricated by a powder metallurgy process [J]. Materials Chemistry And Physics, 2012, 136(2−3): 990−998.
[20] CHANG Y, HUANG D, JIA C, GE C, LIANG D, GAO P. Oxide dispersion strengthened ferritic steel fabricated by mechanical alloying and spark plasma sintering [J]. Powder Metallurgy, 2014, 57(2): 103−110.
[21] YANG Zhan-bing, HU Ben-fu, KINOSHITA H, TAKAHASHI H, WATANABE S. Effect of hydrogen ion/electron dual-beam irradiation on microstructural damage of a 12Cr-ODS ferrite steel [J]. Journal of Nuclear Materials, 2010, 398(1−3): 81−86.
[22] SONG K X, XING J D, DONG Q N, LIU P, TIAN B H, CAO X J. Optimization of the processing parameters during internal oxidation of Cu−Al alloy powders using an artificial neural network [J]. Materials & Design, 2005, 26(4): 337−341.
[23] RAMAN L, GOTHANDAPANI K, MURTY B S. Austenitic oxide dispersion strengthened steels: A review [J]. Defence Science Journal, 2016, 66(4): 316−322.
[24] LIU Ye, QIN Ming-li, ZHANG Lin, JIA Bao-rui, CAO Zhi-qin, ZHANG De-zhi, QU Xuan-hui. Solution combustion synthesis of Ni−Y_2O_3 nanocomposite powder [J]. Transactions of Nonferrous Metals Society of China, 2015, 25(1): 129−136.
[25] KUBENA I, POLAK J, PLOCINSKI T P, HEBERT C, SKORIK V, KRUML T. Microstructural stability of ODS steels in cyclic loading [J]. Fatigue & Fracture of Engineering Materials & Structures, 2015, 38(8): 936−947.
[26] TOUALBI L, CAYRON C, OLIER P, MALAPLATE J, PRAUD M, MATHON M H, BOSSU D, ROUESNE E, MONTANI A, LOGE R, de CARLAN Y. Assessment of a new fabrication route for Fe−9Cr−1W ODS cladding tubes [J]. Journal of Nuclear Materials, 2012, 428(1−3): 47−53.
[27] BECHADE J L, TOUALBI L, BOSONNET S, CASTELNAU O, de CARLAN Y. Macroscopic and microscopic determinations of residual stresses in thin oxide dispersion strengthened steel tubes [J]. Materials Science Forum, 2014, 768−769: 296−303.
[28] OKSIUTA Z, KOZIKOWSKI P, LEWANDOWSKA M, OHNUMA M, SURESH K, KURZYDLOWSKI K J. Microstructural changes upon annealing in ODS-strengthened ultrafine grained ferritic steel [J]. Journal of Materials Science, 2013, 48(13): 4620−4625.
[29] OKSIUTA Z, BALUC N. Optimization of the chemical composition and manufacturing route for ODS RAF steels for fusion reactor application [J]. Nuclear Fusion, 2009, 49(5): 055003(1−9).
[30] ZHOU Shi-meng, CHENG Xing-wang, ZHANG You-jing, WANG Meng, JIANG Wen, CAI Hong-nian. Factors affecting the mechanical properties of ultra-high-strength bainitic steel containing W and 0.33mass% C [J]. Journal of Iron and Steel Research (International), 2016, 23(3): 289−296.
[31] YANG F, SAXENA A, RIESTER L. Use of the nano-indentation technique for studying microstructure/crack interactions in the fatigue of 4340 steel [J]. Metallurgical & Materials Transactions A, 1998, 29(12): 3029−3036.
[32] PHARR G M J. An improved technique for determining hardness and elastic modulus using load and displacement sensing indentation experiments [J]. Journal of Materials Research, 1992, 7(6): 1564−1583.
[33] WANG Jun-sheng. Influence of alloying elements on the elastic modulus [J]. Chinese Journal of Rare Metals, 1979(4): 1−11. (in Chinese)

ZrO_2粒子弥散强化 Q345 钢的制备、显微组织与力学性能

王宝安[1]，王 宁[1,2]，杨玉婧[1]，钟 华[1]，马明臻[1]，张新宇[1]，刘日平[1]

1. 燕山大学 亚稳材料制备技术与科学国家重点实验室，秦皇岛 066004；
2. 中海油炼油化工科学研究院，青岛 266500

摘 要：采用中频感应熔炼炉熔化钢液和喂丝法相结合的技术，将 ZrO_2 粒子与铁粉混合物的预制棒加入到 Q345 钢熔液中，制备不同 ZrO_2 粒子含量(0%、5%和 1.2%，质量分数)的弥散强化 Q345 钢。通过光学显微镜(OM)、扫描电子显微镜(SEM)和透射电子显微镜(TEM)观察铸态、正火态和淬火态弥散强化钢的显微组织和拉伸断口形貌，并分析 ZrO_2 粒子弥散强化 Q345 钢的强化机理和断裂机理。结果显示，ZrO_2 粒子弥散强化 Q345 钢的强度得到显著提高；ZrO_2 粒子附近形成的位错胞以及 ZrO_2 粒子的钉轧作用是弥散强化钢力学性能提高的主要强化机理；另外，硬质马氏体相、晶粒细化和高含量 ZrO_2 粒子在强化过程中均起到重要作用。采用纳米压痕仪对弥散强化钢的硬度和变形能力进行研究。结果表明，ZrO_2 粒子弥散强化 Q345 钢的硬度随 ZrO_2 粒子含量的增加而提高。

关键词：Q345 钢；ZrO_2 粒子；弥散强化；显微组织；力学性能

(Edited by Bing YANG)